Different avulsion events throughout the evolution of submarine channel-levee systems: A 3D seismic case study from the northeastern Bengal Fan

Kun Qi [a,b], Liangbo Ding [c], Chenglin Gong [a,b,*], Haiqiang Wang [c], Dali Shao [c], Zheng Cai [c], Hongxia Ma [c], Xiaoyong Xu [c], Zhenkui Jin [a,b]

[a] *State Key Laboratory of Petroleum Resources and Prospecting, China University of Petroleum (Beijing), Beijing, 102249, China*
[b] *College of Geosciences, China University of Petroleum (Beijing), Beijing, 102249, China*
[c] *PetroChina Hangzhou Research Institute of Geology, Hangzhou, 310023, China*

ARTICLE INFO

ABSTRACT

As very common deep-water phenomena, submarine channel avulsions have been paid considerable attention recently. The differences among them are, however, rarely noted, nor their relationship to the evolution of submarine channels. A seismically well-imaged channel-levee system from the Pliocene Bengal Fan, named target channels (TCs) and consisting of three independent channels (Tc1-Tc3), has been selected as a case to address these issues. Using high-resolution 3D seismic data along with spectral decomposition and RGB color blending techniques, this study images TCs from initiation to abandonment and recognizes three different types of avulsion events: regional avulsion, local avulsion and bank crevasse. In the early evolution stage of TCs, the regional avulsion and the local avulsion successively occurred, promoting TCs to obtain a stable flow course and then undergo a significant evolution. Moreover, coupled with those regional and local avulsion events, TCs were growing respectively in the form of individual channel and amalgamated stacking. In the late evolution stage of TCs, only bank crevasses occurred and led to the formation of crevasse splays in the overbank setting, which coincided with the aggradational stacking of TCs developing. This new evolution model of channel-levee systems, which acknowledges different avulsion events, may provide insights on the understanding of analogue deep-water deposits and in turn can be applied to guide the hydrocarbon exploration and development.

1. Introduction

Avulsion of submarine channels has long been recognized in deep-water systems (Damuth et al., 1983a; b; Kolla and Coumes, 1987; Manley and Flood, 1988; Flood et al., 1991). On the Amazon Fan (Pirmez et al., 1997), the Zaire Fan (Droz et al., 2003), the Indus Fan (Kenyon et al., 1995), and the Bengal Fan (Curray et al., 2003), submarine channel avulsions frequently occurred, controlling the distribution of channel sands, lobe sands, and therefore the evolution and growth of submarine fans (Piper and Normark, 1983; Piper and Normark, 2001; Primez and flood, 1995; Ortiz-Karpf et al., 2015; Hodgson et al., 2018).

Previous studies on submarine channel avulsions have mainly focused on the occurrence of avulsion processes (Armitage et al., 2012; Zhao et al., 2018a), the temporal-spatial distribution of avulsion nodes (Kolla, 2007; Picot et al., 2016, 2019), and the relationships between avulsions and topographic conditions (Clark and Cartwright, 2009; Ortiz-Karpf et al., 2015; Howlett et al., 2019). However, few studies have paid attention to the presence of differences within those commonly occurred avulsion events (Zhao et al., 2019; Lowe et al., 2019). Although in most cases avulsions can be large-scale events where the diverted flows totally change the flow direction of channel courses (Piper and Normark, 2001; Kolla, 2007), they sometimes can also be of local nature that the avulsive new channel rejoins its parent channel downstream (Maier et al., 2013; Zhao et al., 2018b). Moreover, in some extreme cases, avulsive flows diverted out of an established channel tend to directly deposit their sediments in the overbank area to form a crevasse splay instead of initiating a new channel course (Posamentier and Kolla, 2003; Lowe et al., 2019). Those three different types of submarine channel avulsions can be defined from the fluvial realm
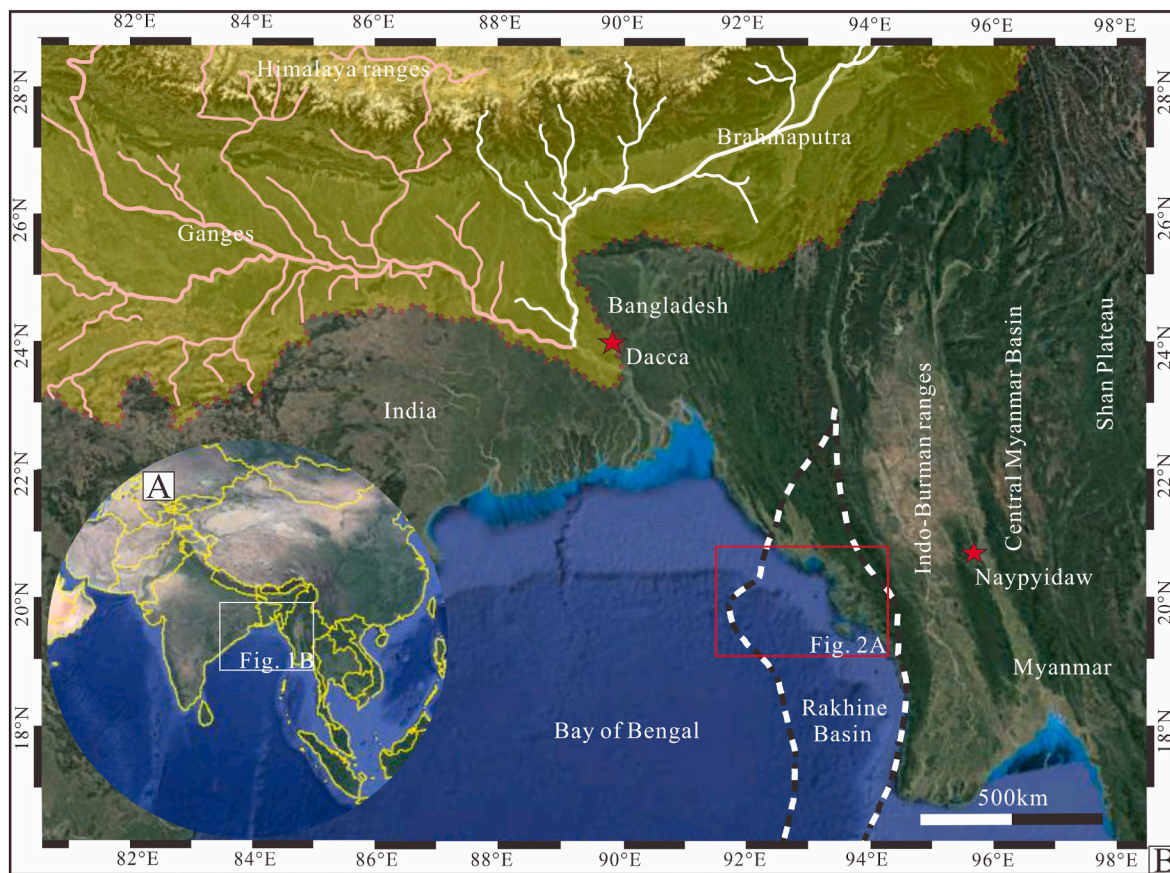

Fig. 1. (A) Geographic context of the study area around the Bay of Bengal. (B) Physiography of the Ganges-Brahmaputra source-to-sink system, from the catchment to the deep-sea fan. The studied submarine channels are in the northeastern Bengal Fan (red rectangle) and mainly fed by terrigenous sediments transported by the Ganges and Brahmaputra rivers. The Rakhine Basin and several main tectonic provinces in the east, including the Indo-Burman ranges, the Central Myanmar Basin, and the Shan Plateau, are also shown. (For interpretation of the references to color in this figure legend, the reader is referred to the Web version of this article.)

(Smith et al., 1989; Heller and Paola, 1996; Slingerland and Smith, 2004) and they are termed as 'regional avulsion', 'local avulsion' and 'bank crevasse' respectively. Previous studies have never recognized such different avulsions collectively occurring in one submarine channel-levee system, nor related them to the overall evolution of submarine channels.

The present study takes submarine channels from the late-Pliocene Rakhine Basin, northeastern fringe of the Bengal Fan as study objects. They are informally named "target channels" (abbreviated as TCs). Because submarine channels of Bengal Fan are associated with the world's largest fluvio-deltaic system (i.e., the Bengal Delta) and the world's largest orogenic system (i.e., the Himalayan Range) (Curray, 1991; Curray; Munasinghe, 1991; Alam et al., 2003), they have great research value and have been documented by considerable studies (Sun et al., 2011; Yang and Kim, 2014; Harrowfield, 2015). Based on high-resolution seismic data, this study conducts a three-dimensional seismic anatomy for TCs to investigate the different avulsion phenomena throughout the evolution of submarine channel-levee systems. Specifically, we first (1) recognize and characterize the different avulsion events occurred in TCs, then (2) relate them to different channel-evolution stages and associated architectural characteristics, and finally (3) establish a new generic model of channel-levee systems that takes the chronological development of avulsion events and the resulting implications into account. These new insights can be applied to hydrocarbon exploration and development in analogue submarine-channel deposits.

2. Geological background

The study area is located within the offshore Rakhine Basin, the northeastern fringe of the Bengal Fan (Fig. 1). As the largest fan system in the world (Curray and Moore, 1971; Curray et al., 2003), Bengal Fan initiated and developed in response to the collision between Indian and Eurasian plates and consequent Himalayan uplift and denudation since the early Eocene (Curray, 1994; Weber et al., 2003). The plate collision and subsequent orogeny facilitated voluminous clastic detritus that were transported into the Bay of Bengal through the Ganges and Brahmaputra river systems (Curray, 1991; Alam et al., 2003) (Fig. 1). Generally, Bengal Fan underwent two main stages of tectonic-stratigraphic evolution, namely an initial rifting stage from early Eocene to middle Eocene and a post-rifting stage from late Miocene to Holocene (Bastia et al., 2010). The studied TCs occurred in the upper Pliocene (Fig. 2) and are constrained by two regional surfaces: T20 and T21 as shown in Fig. 3. Those two horizons could be traced throughout the study area and exactly correspond to the upper and lower boundaries of the upper Pliocene, as shown in previous works on deep-water systems offshore Rakhine Basin (Zhan et al., 2019; Ma et al., 2020).

Specifically, our study area is defined by a 900 km² 3D seismic volume located in the central Rakhine Basin of the Myanmar continental margin (Figs. 1B and 2A). The northeastward oblique subduction of Indian plate beneath the Burmese microplate (Fig. 2B) triggered the formation of N–S trending structural terrains, encompassing from East to West a plateau (Shan Plateau), an arc-related basin (Central Myanmar Basin), and an accretionary prism (Indo-Burman ranges and the Rakhine Basin) (Yang and Kim, 2014; Ma et al., 2020) (Fig. 1B). The Indo-Burman ranges are the eastern boundary of the Rakhine Basin and
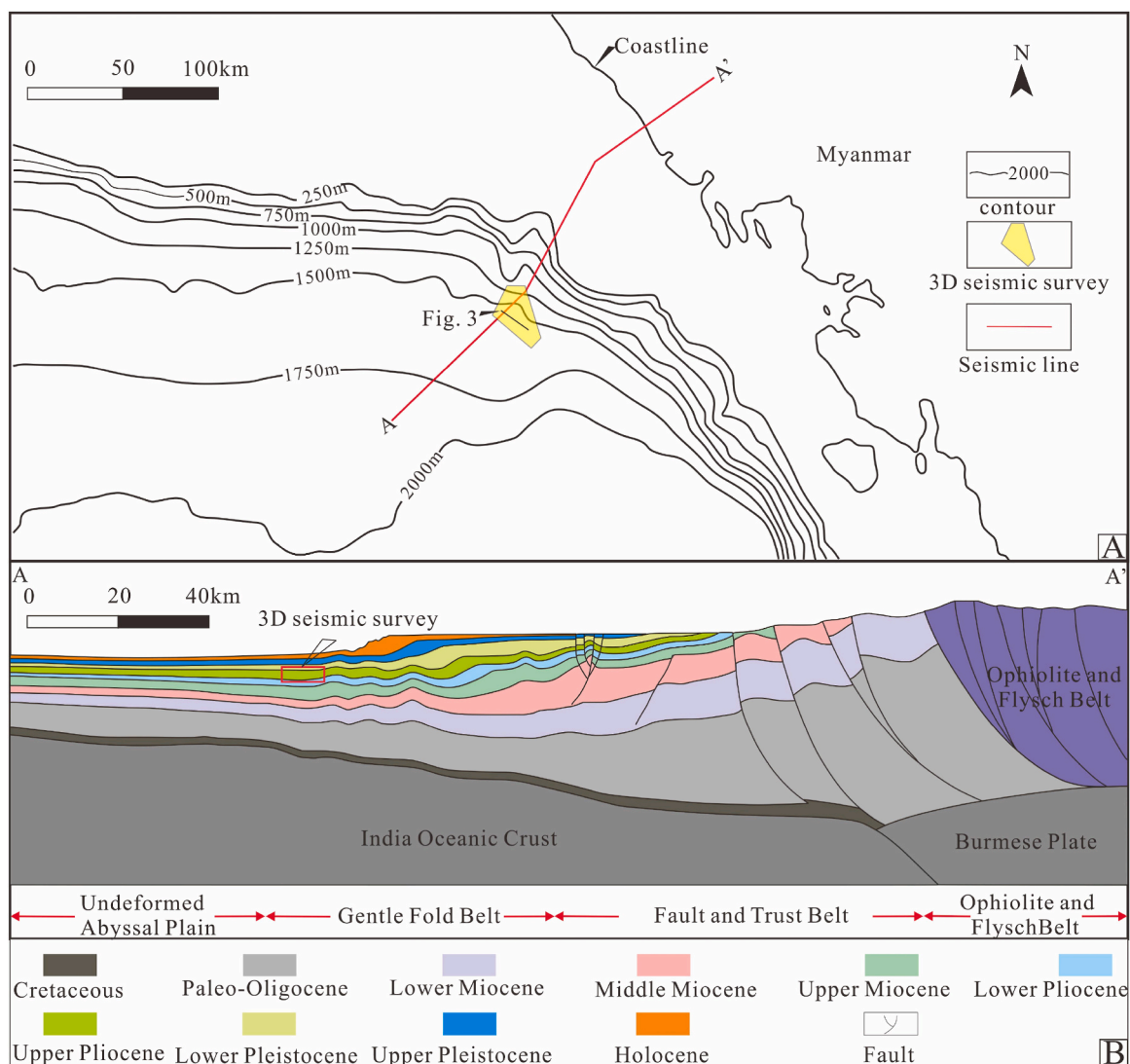
Fig. 2. (A) Bathymetric map of the northeastern fringe of the Bay of Bengal. Locations of the 3D seismic survey, a NE-SW trending regional section, and a seismic line in 3D seismic survey are shown. (B) Regional sketch section across the northern Rakhine Basin. Based on the tectonic deformation intensity, three structural belts are divided: fold and thrust belt, gentle fold belt, and undeformed abyssal plain belt from east to west. Note that the 3D seismic survey used in this study lies in the distal part of the Gentle Fold Belt and that the interval of interest belongs to the Upper Pliocene.

contain flysch deposits, ophiolites (Fig. 2B), and some Eocene turbidite sands, which are suggested to represent early Bengal fan sediments offscraped in the east-dipping subduction zone and uplifted into the accretionary prism (Alam et al., 2003; Curray et al., 2003). Such compressional tectonic forces caused by the plate collision continued throughout the evolution of Rakhine Basin and caused ongoing westward depocenter migration on millennial timescales (Schwenk and Spieß, 2009; France-Lanord et al., 2014). Moreover, the associated tectonic deformation progressively decreased towards the offshore area, forming from East to West three structural belts in the Rakhine Basin, including the fold and thrust belt, the gentle fold belt, and the undeformed abyssal plain belt (Wang et al., 2013; Tang et al., 2013) (Fig. 2B). The TCs and the associated 3D seismic survey lie in the distal part of the gentle fold belt (Fig. 2B).

3. Datasets and methodology

3.1. 3D seismic database

The primary dataset utilized in this study is a 3D seismic data that occupies an area of around 900 km^2 (Fig. 2A). It was acquired in 2012 by the China National Petroleum Corporation (CNPC) and is a Kirchhoff Post Stack Depth Migrated (PSDM) volume. The data has a dominant frequency of 30 Hz, a bin size spacing of 25 m by 12.5 m and a sampling rate of 2 ms. It was displayed using the SEG negative standard polarity, where a positive reflection coefficient corresponds to an increase in acoustic impedance, and is represented by a positive/peak reflection event (red in color).

3.2. Seismic data interpretation

Two main steps were employed to analyze the TCs: (1) The definition of the seismic (isochronous) stratigraphic framework for the interval of interest and (2) the utilization of seismic transects and attribute maps to characterize the avulsion and growth of TCs. The establishment of stratigraphic framework is mainly based on the modeling capability of PaleoScan Software; a horizon stack containing a number of isochronous surfaces was created and totally six horizons (named slice1 to slice 6 from oldest to youngest) were selected to define the study interval (Fig. 3A). For individual horizons, RMS-amplitude attribute maps and the associated red-green-blue (RGB) color blends were extracted from the 3D seismic volume to document the seismic geomorphology of TCs.
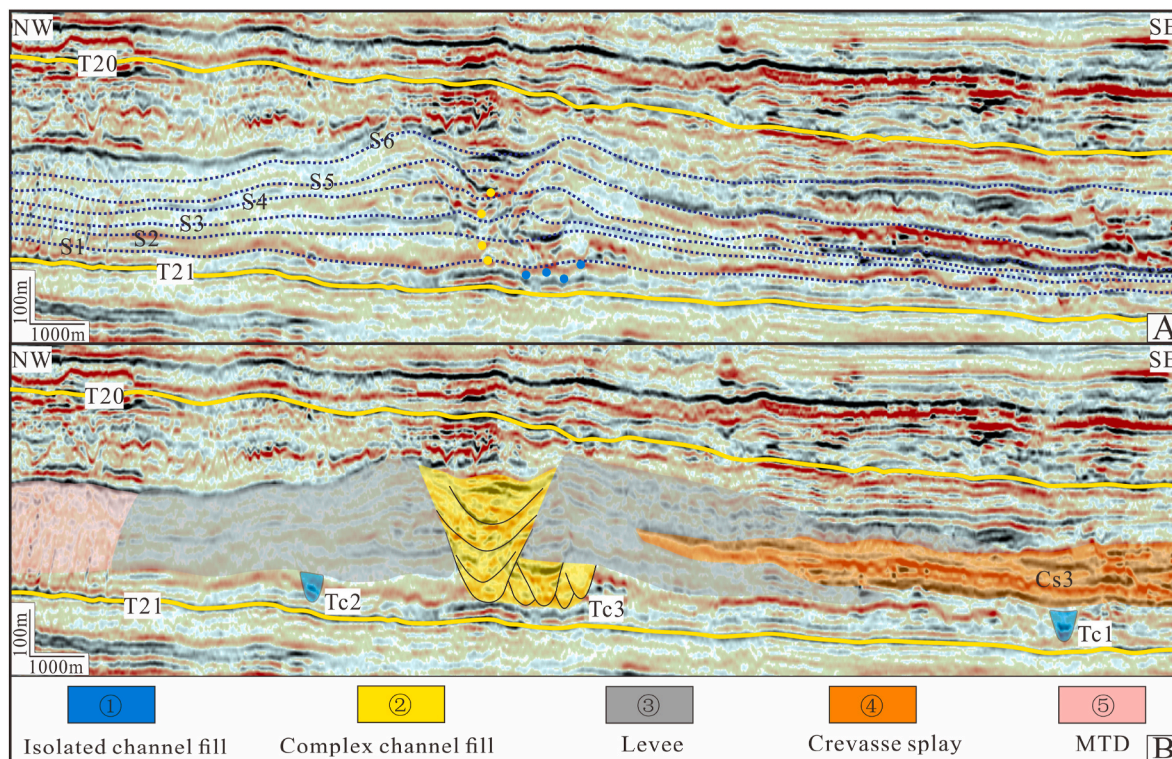
Fig. 3. A typical seismic section (uninterpreted and interpreted for A and B) showing the seismic stratigraphy in the study area and the five kinds of seismic facies documented in the interval of interest. In total, six isochronous slices are extracted from the target channels and they are involved with different seismic facies from the bottom to the top. Also, noted that this cross-section is across one crevasse splay (Cs3), which lies on the east bank, thickening away from the channel, and sandwiched by levee deposits (only the most distal part being exposed).

In RGB color blend maps, each color corresponds to a specific frequency, which significantly enhances the visualization of facies distribution and hence inference of depositional processes. In addition, the analysis of planform geometry and amplitude variations on attribute maps are integrated with the cross-sectional seismic facies analysis. Seismic facies represent different elements of the deep-water sedimentary systems, and they are mainly recognized and defined by the configurations of reflectors (reflection continuity and amplitude), cross-sectional geometries, and strata terminations.

Table 1
Tabulation of defined seismic facies in the study interval as observed in cross sections and on seismic attribute (spectral decomposition-RGB blend) maps.

| Seismic facies/Reflection character	Reflection geometry	Seismic cross-section	RGB blend map
① **Isolated channel fill**: Semi-parallel high amplitude reflections	V-shaped channel form with distinct basal surface. Up to c. 90 m height, width c. 0.5 km, > 60 km length		
② **Complex channel fill**: Discontinuous variable (low to high) amplitude reflections	U-shaped deposits consisting of multiple stacked channel forms Up to c. 300 m thickness, width c. 2.8 km, > 40 km length		
③ **Levees**: Low-amplitude, sub-parallel and semi-continuous reflections	Gull wing to wedge shaped taper forms, thinning away laterally Up to 270 m thickness, max. c. 10 km width		
④ **Crevasse splays**: High-amplitude reflection packages, sub-parallel and continuous	Sheet to mounded morphology and commonly occurring on facies ③ Up to c. 180 m thickness, c. 60 km² area		
⑤ **MTDs**: Variable (low to high) amplitude, chaotic reflections	Erosive basal surface, some interval thrusts and mounds		
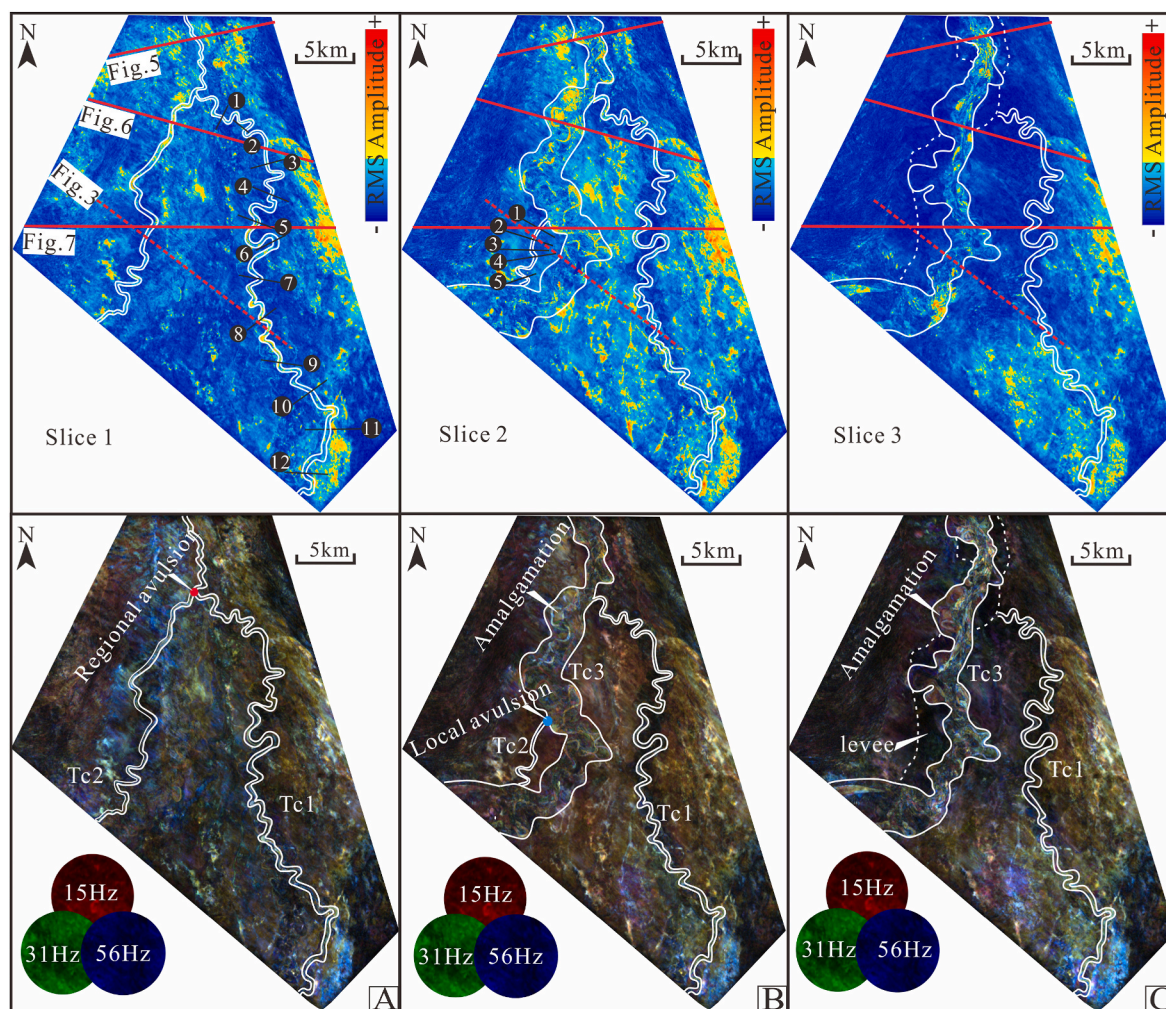
Fig. 4. RMS attribute maps and the associated spectral decomposition RGB color blends of first three isochronous slices, i.e. Slice 1–3 shown in Fig. 3A. (A) Slice 1 showing the avulsion of Tc2 from west bank of Tc1, which directly results in the abandon of the parent channel (Tc1) and the change of flow course on a regional scale. (B) Slice 2 showing subsequently Tc3 avulsed from the east bank of Tc2 and then rejoined it downstream, which only results in the abandonment of the parent channel (Tc2) and the change of flow course on a local scale. Noted that Tc3 had gone through a significant evolution after avulsion and presented a distinct amalgamated architecture pattern (C) Slice 3 showing Tc3 persistently developed and the associated levee deposits (bounded by dashed lines) started to show up locally to obscure the abandoned segment of Tc2 and the headwall domain of Tc1. (For interpretation of the references to color in this figure legend, the reader is referred to the Web version of this article.)

3.3. Quantitative indicators of TCs

Morphometric parameters (including width, height and sinuosity) were employed herein to quantify morphometric properties of the TCs. Along the main pathways, channel widths and heights are measured in a series of cross-sections that are extracted perpendicular to the overall flow direction. The sinuosities of submarine channels represent the ratio of the along-channel length over the straight-line distance between the start and end points of the window segment. Hence, their values depend heavily on the lengths of segments chosen for measuring (Ferry et al. 2005; Clark and Cartwright, 2011), and we herein employed a step length of 5 km as the sliding window of sinuosity measurements. Moreover, the kinematic and architectural characteristics of the TCs are quantified by the channel-trajectory angle (A_c), computed by:

$A_c = \arctan (dy/dx)$ (Gong et al., 2017).where dx and dy are respectively the lateral and vertical components of a specific channel-migration pathway, which consists of two adjacent channel forms. High values of A_c generally correlate to aggradational channel successions, whereas low values usually correspond to amalgamated patterns.

4. Seismic facies and corresponding depositional elements

4.1. Description of seismic facies

Within the study interval, we define five dominant seismic facies (Seismic facies 1 through 5) based on the integration of cross-sections and seismic attribute maps (Fig. 3 and Table 1). Seismic facies 1 and 2 contain similar defining characteristics; they are both characterized by V-shaped or U-shaped confinements in cross sections and high-sinuosity threads in map view (Fig. 3 and Table 1). However, those two facies show significant differences in terms of scales; facies 1 have relatively larger widths (up to 2.8 km) and heights (up to 300 m) compared with those of facies 2 (with widths up to 0.5 km and heights up to 90 m) (Table 1). Seismic facies 3 collectively occur on either side of facies 2 strata. They are composed of low-amplitude, semi-continuous reflectors that form gull-wing to wedge-shaped packages (Fig. 3 and Table 1). Furthermore, facies 3 have a maximum thickness of 270 m and extend laterally for around 10 km, almost 3 times of the corresponding facies 2 widths (Table 1).

Seismic facies 4 are characterized by sub-parallel, continuous, and high-amplitude reflection packages that are sheet to mounded in cross-
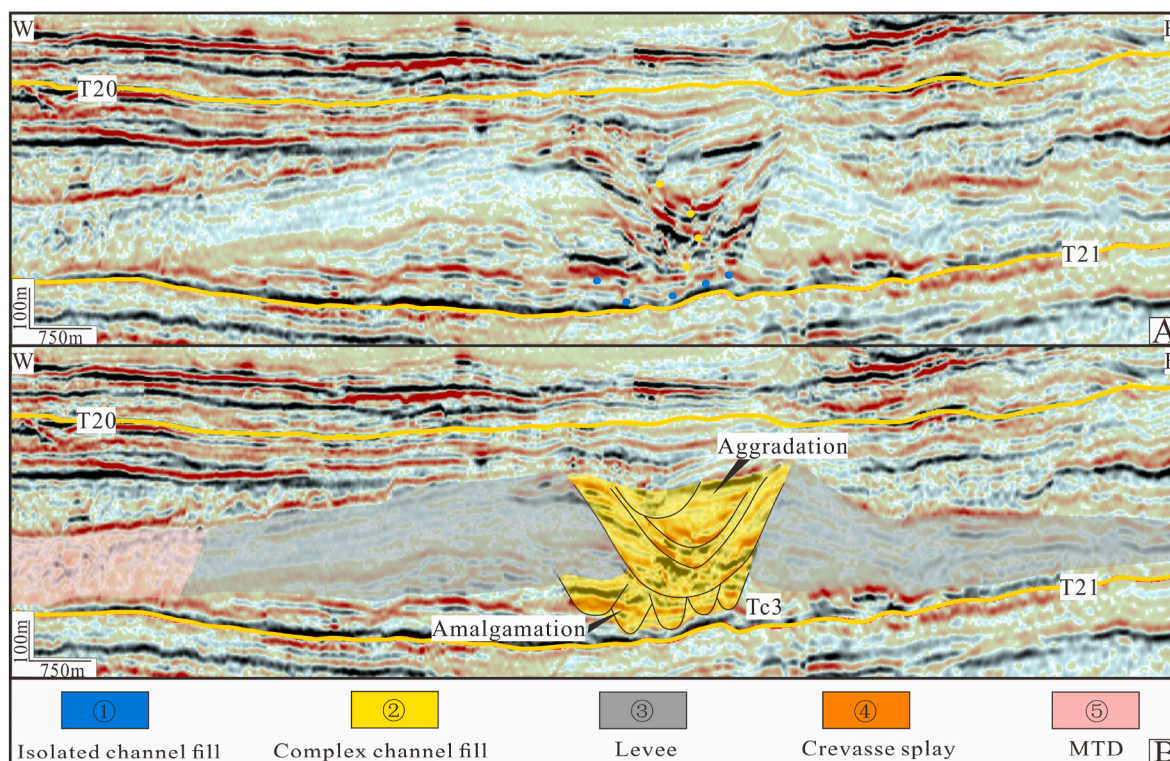
Fig. 5. Uninterpreted (A) and interpreted (B) seismic cross-sections across the upstream segment of target channels (see Fig. 4 for positions on map). Note that because the pre-existing Tc1 and Tc2 had been totally masked by the continuous development of Tc3, at this part only Tc3 is present. Also, Tc3 shows a clear variation in architecture pattern from lateral amalgamation to vertical aggradation, which could also be seen in every seismic sections presented in this study.

section and lobe-shaped in map view (Fig. 3 and Table 1). They have a maximum thickness of 180 m and spread for an area up to 60 km^2 (Table 1). Seismic facies 5 consist of variable amplitude, chaotic reflections. Moreover, they collectively have erosional bases and irregular tops and show thrust-like features internally (Fig. 3 and Table 1).

4.2. Interpretation of seismic facies

Because of the absence of well-based and lithological calibration within the study area, the interpretation of seismic facies in this work are carried out through the comparison of the documented seismic facies with previous studies of deep-water systems. Seismic facies 1 and 2 showing distinct V- to U-shaped confinements are commonly interpreted as submarine channel fill deposits (Abreu et al., 2003; Posamentier and Kolla, 2003; Deptuck et al., 2007; Hansen et al., 2017; Gong et al., 2020). The reason we divided them into two different facies is that they belong to different hierarchies. Seismic facies 1 consist of only one channel element and is relatively small in scale, while facies 2 consist of stacked complexes of channel elements and have relative larger scales (Fig. 3, Table 1). Therefore, we here interpret those two facies respectively as isolated channel fills and complex channel fills (Table 1, Fig. 3). Seismic facies 3 constructed on either side of channel fills are considered as levees (Deptuck et al., 2003; Nakajima and Kneller, 2013; Oluboyo et al., 2014) (Table 1, Fig. 3); they form an important stratigraphic component of many deep-water systems and generally have relatively large scales and fine-grained deposits.

In deep-marine environments, the splay deposits (i.e. seismic facies 4) overlying on levees and laterally connected with channel fills are generally considered as crevasse splays (Posamentier and Kolla, 2003; Ortiz-Karpf et al., 2015); they are deposited from unconfined gravity flows originating from levee breaches (Table 1, Fig. 3). Seismic facies 5 with chaotic reflections are commonly thought to represent mass-transport deposits (MTDs) (Moscardelli et al., 2006; Bull et al., 2009; Gong et al., 2014) (Table 1, Fig. 3). Though occupying a large part

of the study area, those MTDs has nothing to do with the avulsion and evolution of TCs and thus are not considered in this study.

5. Different avulsion events of TCs

In the study area, TCs consist of three independent submarine channels, respectively named Tc1, Tc2 and Tc3 from chronologically oldest to youngest (Fig. 4). They have undergone different submarine channel avulsions, as discussed below.

5.1. Regional and local avulsion events

As the oldest channel documented in this study, Tc1 trends in a southeasterly direction (Fig. 4). Its associated avulsion events occurred at an outer channel bend in the very upstream segment (the red dot in Fig. 4A), which took the entire flow discharge of the parent channel (Tc1) and gave rise to the formation of a new channel, i.e. Tc2. Because the avulsion event caused the abandonment of Tc1 down-dip of the avulsion site and fully changed the flow direction from southeast to southwest, it is thought to be a regional process and thus, termed as 'Regional avulsion' (Fig. 4A). Following this, another avulsion event occurred in the downstream segment of Tc2 (the blue dot in Fig. 4B). Different from the previous regional process that had caused the formation of a completely new course, the newly avulsed channel, i.e. Tc3, reoccupied the older Tc2 immediately downstream, giving the appearance of channel merger or confluence (Fig. 4B). Tc3, therefore, overlapped the major segments of Tc2 and only a small part of Tc2 was abandoned during the avulsion (Fig. 4B). Therefore, the associated avulsion event is of local nature and termed "Local avulsion" (Fig. 4B).

Although those avulsion events had caused the abandonment of the parent channel, the overlapping parts among these three channels, i.e. the segments up-dip of avulsion sites and down-dip of the confluence sites, were still active conduits and parts of Tc3. Because Tc3 had gone through a significant evolution after its inception, the overlapping
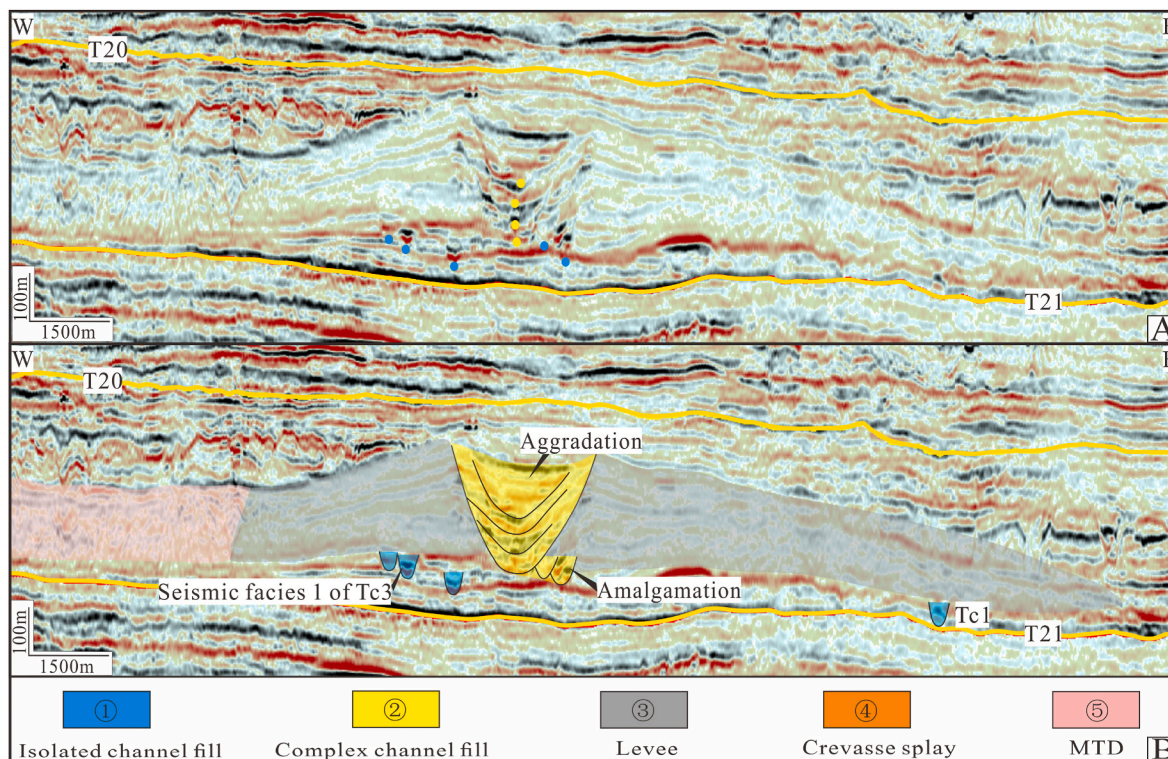
Fig. 6. Uninterpreted (A) and interpreted (B) seismic cross-sections across the midstream segment of target channels (see Fig. 4 for positions on map). Note that in this section Tc3 and the abandoned parts of Tc1 could be recognized, while the Tc2 is not preserved due to the continuous development of Tc3. Occurred at an earlier time, Tc1 is overlain by the levee deposits of Tc3 and has a much smaller scale compared with the latter. On the other hand, note that within the amalgamated channel succession of Tc3, the lateral-offset amount of channel elements could be very large, giving rise to the formation of isolated channel fills (Seismic facies 1) locally.
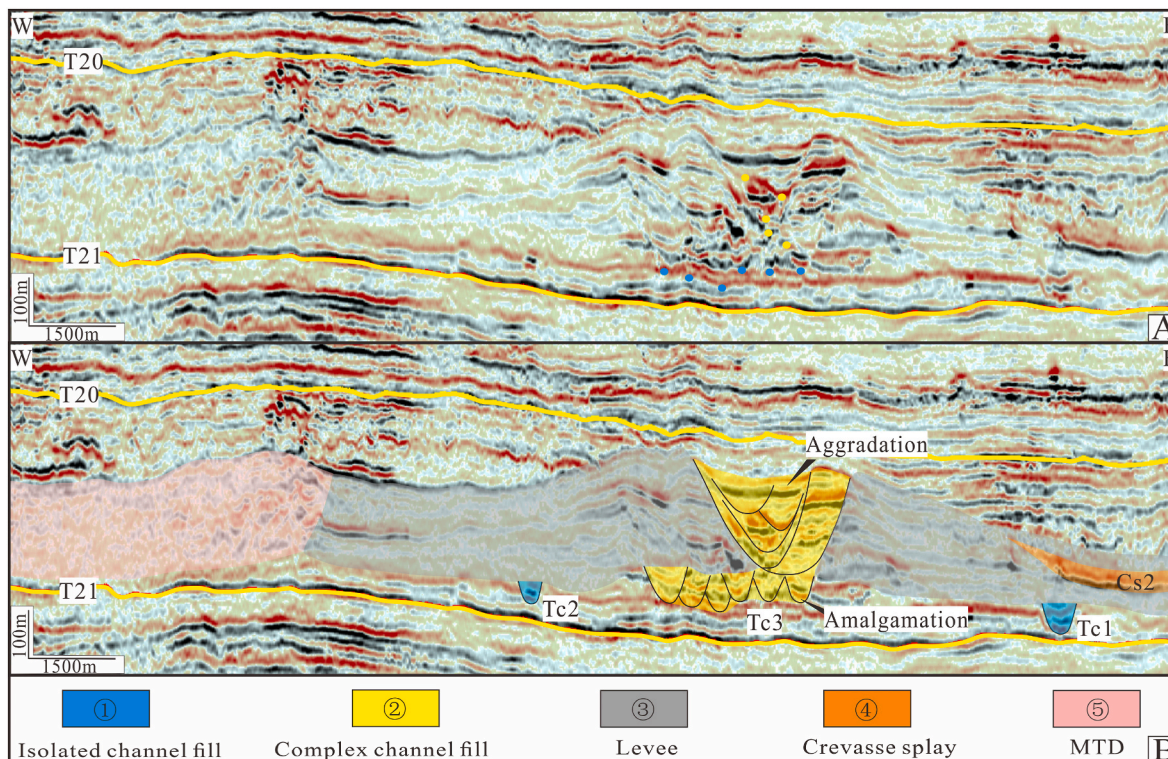

Fig. 7. Uninterpreted (A) and interpreted (B) seismic cross-sections across the downstream segment of target channels where Tc1, Tc2, and Tc3 are all presented (see Fig. 4 for positions on map). Note that the early-formed Tc1 and Tc2 are both overlain by the levee deposits of Tc3 and they have much smaller scales compared with Tc3. Also shown is a very small part of a crevasse splay (Cs2) occurred at a later time of channel evolution.
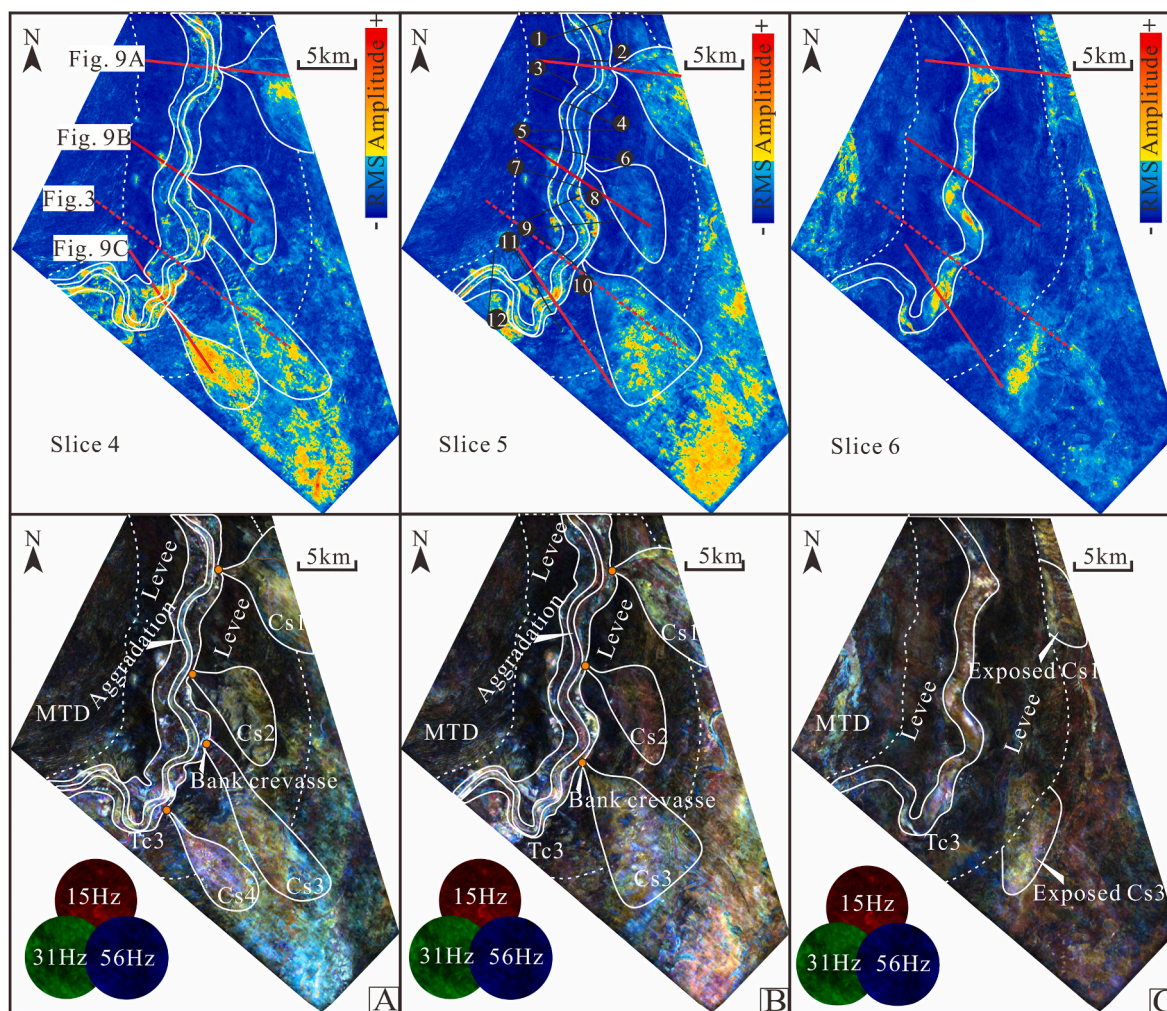
Fig. 8. RMS attribute maps and the associated spectral decomposition RGB color blends of last three isochronous slices, i.e. Slice 4–6 shown in Fig. 3A. (A) Slice 4 showing the occurrence of four times of levee breaching on the east bank of Tc3, which had caused the formation of four corresponding crevasse splays (Cs1–Cs4). (B) Slice 5 showing with the evolution of Tc3, the most-downstream levee breach had sealed and the corresponding crevasse splay had been draped by the subsequent levee deposits. (C) Slice 6 showing in the final stage of channel evolution, the residual three levee breaches became sealed and their corresponding crevasse splays were also overlain by the overbank deposits, with only small parts of Cs1 and Cs3 being exposed. In addition, note that during the evolution stage shown in these three slices, the earlier formed Tc1 and Tc2 were totally obscured by the levee deposits of Tc3, and that the architecture pattern of Tc3 turned to be vertical aggradation from the early lateral amalgamation shown in Fig. 4. (For interpretation of the references to color in this figure legend, the reader is referred to the Web version of this article.)

segments of Tc1 and Tc2 had long been used and modified by the subsequently formed Tc3 and inherited the general characteristics of it (Fig. 4B and C). Therefore, we here classified those reaches as a part of Tc3 where Tc1 and Tc2 cannot be distinguished in cross-sections but only in the profiles that across the abandoned segments (Figs. 3, 5, 6, and 7). Furthermore, these abandoned segments of Tc1 and Tc2 were gradually overlain by the constructed levee deposits of Tc3 and become obscured in isochronous slices (Figs. 4C and 8).

5.2. Bank crevasse and resultant crevasse splays

Different from the early Tc1 and Tc2, which only were active for a short duration due to the occurrence of avulsion, Tc3 persistently developed after its avulsive initiation and constructed pronounced levee deposits, as bounded by the dashed lines in Figs. 4 and 8. Therefore, the associated avulsion events of Tc3 have directly resulted from the breaching of levees and in total four breaches are recognized in this study (orange dots in Fig. 8A). On the one hand, avulsive flows originating from those breaches did not initiate the formation of new channel courses but only formed distinct crevasse splay deposits in the proximal

overbank setting (Fig. 8A). On the other hand, with ongoing channel evolution, those levee breaches did not deepen or enlarge to take more flow discharge of Tc3 but gradually healed to prevent any further flows (Fig. 8B-C). Furthermore, after theses breaches were fully sealed, the levee deposits continuously developed on top of the crevasse splays, as shown in a series of seismic sections that cross four splay deposits (Figs. 3 and 9). Above all, it could be found that the avulsion events of Tc3 did not have any impact on the shifting of flow courses and thus, are termed 'bank crevasses' (Fig. 8).

In total, four crevasse splays are recognized in this study and they are respectively named Cs1 to Cs4 along the entire length of Tc3 (Fig. 8). Moreover, these four splay deposits share a lot in common; they are collectively occurred at the east channel bank, sandwiched by the levee deposits, and characterized by a thickening trend laterally, (Figs. 3, 8 and 9). Specifically, Cs1 is distributed in the northeastern part of the seismic survey and assumed a lobate shape; it has an extension area of 31.93 km^2 and a maximum thickness of 182 m, with the most distal part not being draped by levee deposits. (Figs. 8 and 9A). Cs2, located in the south of Cs1, also presents a lobate shape, with an area of 41.39 km^2 and a maximum thickness of 95 m (Figs. 8 and 9B). Cs3 is the largest crevasse
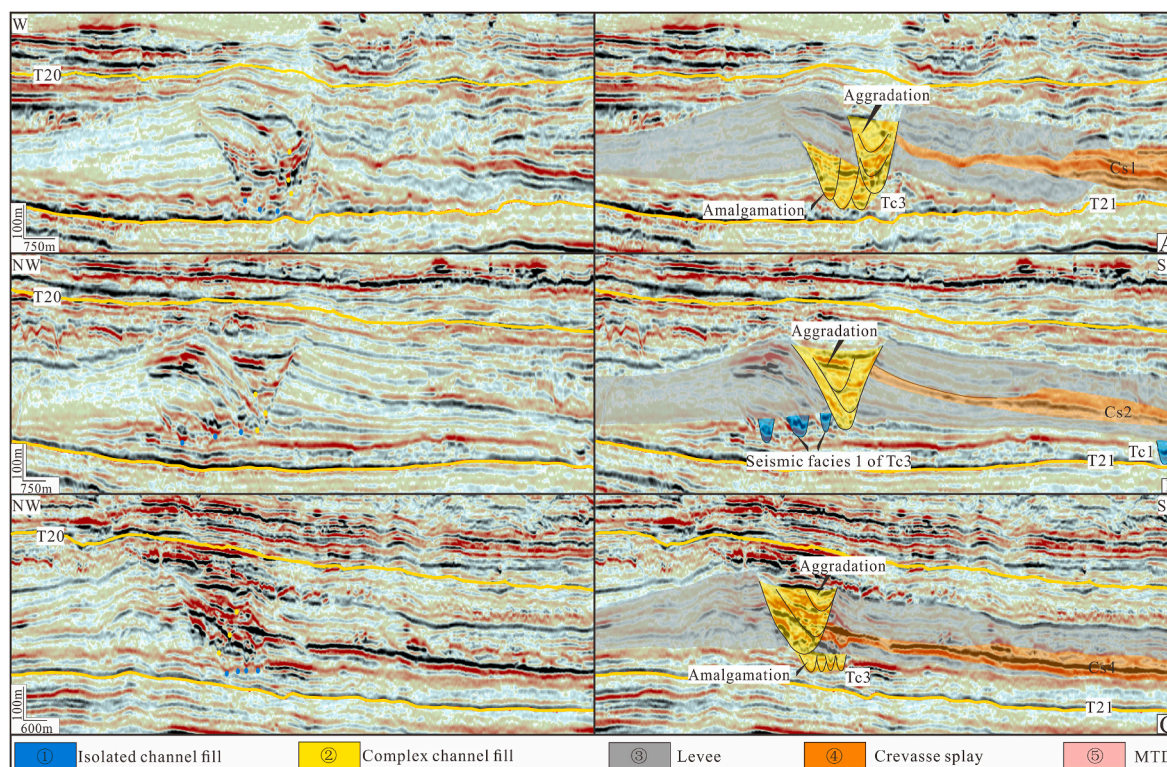
Fig. 9. A series of uninterpreted and interpreted seismic sections across the Cs1 (A), Cs2 (B) and Cs4 (C). It can be seen that all those crevasse splays occurred when the channel elements in Tc3 stacked in an aggradation pattern and that they are all sandwiched by the levee deposits of Tc3, with only a small parts of Cs1 being exposed. Moreover, these crevasse splays collectively show a thickening trend laterally in cross-sections.

Table 2

Architectural characteristics of three independent submarine channels in the present study.

Channel	Along-channel distance (km)	Width range/Mean (m)	Height range/Mean (m)	Constitution
T1C1	62.04	211-422/ 332	55-90/70	Seismic facies 1
T1C2	8.27	246-302/ 281	50-67/62	Seismic facies 1
T1C3	44.79	2197-3051/ 2688	267-378/292	Seismic facies 1, 2 and 3

splays documented in this work; it shows an elongated shape, with an area of 62.65 km^2 and a maximum thickness of 145 m (Figs. 3 and 8). Cs4 has an elliptical shape and the smallest size, with an area of 29.03 km^2 and a maximum thickness of 77 m. Furthermore, Cs4 is the first one to be draped by accumulated levees after the breach was sealed (Figs. 8B and 9C).

6. Architectural characterization of TCs

There are significant differences among target channels Tc1, Tc2, and Tc3. To better understand their development, it is crucial to quantify the architectural characteristics of these three channels, including the morphometrics and the internal stacking patterns.

6.1. General description of TCs

In the initial evolution stage of TCs, Tc1 occurred at the eastern part of the seismic survey and only consists of seismic facies 1, i.e. isolated channel fills (Fig. 3 and Table 2). It extends southeastward for about 62 km and has widths of 211–422 m and heights of 55–90 m, respectively

averaging 332 m and 70 m (Fig. 10, Table 2). Moreover, Tc1 shows a high-sinuosity character in map view, and the sinuosities are measured to be 1.13–2.17, with an average value of 1.56 (Fig. 4).

Tc2 avulsed from a sharp bend in Tc1 and also only consists of seismic facies 1 (isolated channel fills) (Fig. 3 and Table 2). Because most parts of Tc2 had been modified by the formation of Tc3, only the small abandoned segment (about 8.27 km) is measured for cross-sectional parameters (Fig. 4A and B). The results show that Tc2 has widths of 246–302 m and heights of 50–67 m, respectively with an average value of 281m and 62m, which are comparable with those of Tc1 (Fig. 10 and Table 2).

Tc3 went through a significant evolution after avulsing from Tc2. Hence, it has continuously developed complex channel fills (seismic facies 2) and levee deposits (seismic facies 3) (Fig. 3, Tables 1 and 2). Moreover, in some extreme cases the lateral-offset of channel elements within seismic facies 2 can be very abrupt, resulting in isolated channel fills (seismic facies 1) locally (Figs. 6 and 9B). Extended for about 45 km, the cross-sectional parameters of Tc3 are one order higher than those of Tc1 and Tc2; it has widths between 2197 m and 3051 m and heights between 267 m and 378 m, respectively with an average value of 2688m and 292 m (Fig. 10 and Table 2).

6.2. Architectural style of TCs

According to the differences in morphometrics and constitutions among three independent channels, it was found that Tc3 accounted for the majority of TCs, and that before Tc3 came out, there is a period when channels existed in the form of individual channels (Tc1 and Tc2). Furthermore, the channel fills of Tc3 consist of many channel elements deposited from multi-stage gravity flows. Generally, these internal channel elements could be further divided into two discrete populations: 1) the amalgamated succession within the lower fill level and 2) the aggradational succession in the upper fill level. Therefore, it could be
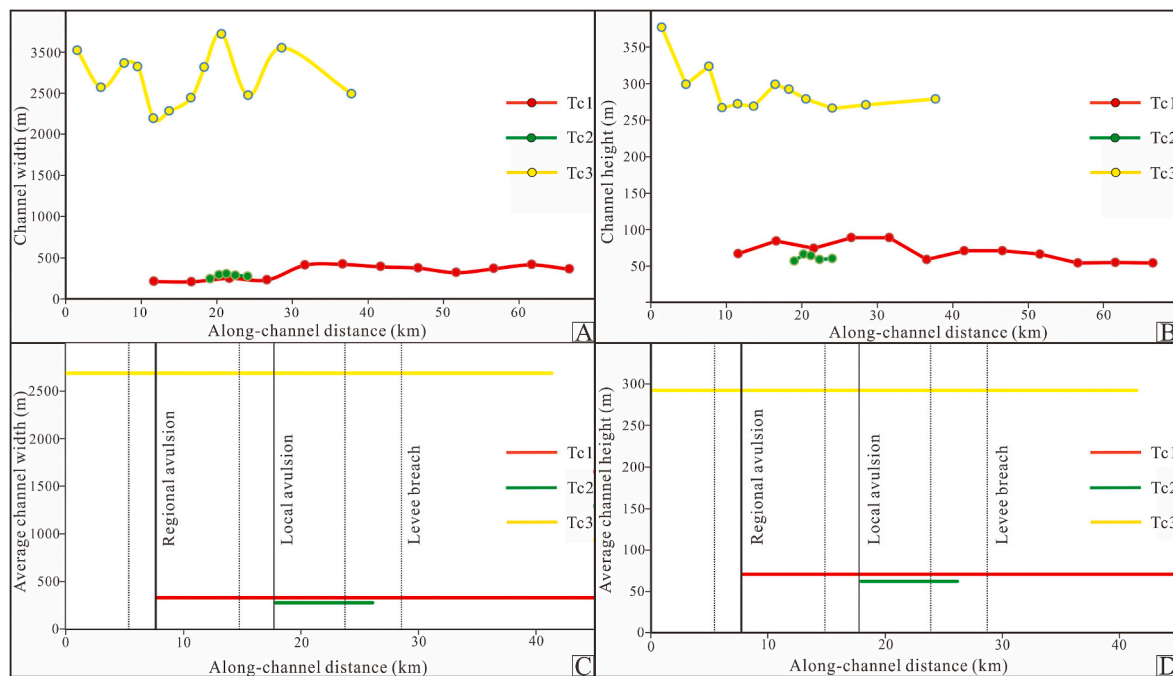
Fig. 10. Quantitative analyses of Tc1, Tc2 and Tc3 showing their down-channel changes in widths (A) and heights, (B) and the corresponding average values (C–D). Note that Tc1 and Tc2 are comparable in size, but both of them are rather smaller than Tc3. The x-axis in this figure refers to the distance along the main path of Tc3, with the origin respresenting the northernmost limit of the seismic survey. All presented data points are measured from a series of sections that are perpendicular to the flow direction, as shown in Figures, 4A, 4B and 8B. The spacial distribution of avulsion events (including regional avulsion, location avulison and bank crevasse) are also shown by vertical solid or dashed lines.

concluded that during the evolution process, TCs underwent a transition in architectural styles from individual channel through amalgamated stacking to aggradational stacking.

The amalgamated channel succession corresponds to a channel kinematics referred to as lateral channel trajectory (blue dots in the seismic sections), which reflects the high magnitude of lateral offset and low amount of vertical accretion from one channel element to the next. Such amalgamated elements have lateral components (dx) of 214–1686 m (averaging 511 m) and vertical components (dy) of 1–52 m (averaging 19.3 m), giving rise to relatively low channel-trajectory angle (Ac) of 1° to 8° (averaging 3°) (Fig. 11). In addition, it could be found from attribute slices (Fig. 4B and C) that the architecture and location of each amalgamated element bears little resemblance to others, thereby showing a disorganized pattern. The shifts of these elements on the seafloor are complex processes and can occur either gradually or abruptly, the latter of which explains the local occurrence of isolated channel fills (Seismic facies 1) within Tc3 (Figs. 6 and 9B).

The aggradational channel succession corresponds to channel kinematics referred to as vertical channel trajectory (yellow dots in seismic sections), where channel elements vertically stacked with minor lateral migration amount. Such aggradational elements have dx of 9–631 m (averaging 181 m) and dy of 25–84 m (averaging 50 m), resulting in relatively high Ac of 4° to 81° (averaging 29°) (Fig. 11).

7. Discussion

7.1. Relating different avulsion events to the overall evolution of submarine channels

According to the abovementioned descriptions, regional avulsion, local avulsion, and bank crevasse sequentially occurred during the evolution process of TCs, among which the first two took place in the early stage (Fig. 4), while the last came up in the late period (Fig. 8). To investigate the specific roles of these avulsion events on the overall channel evolution, we should analyze the essence of both avulsion

behaviors and channel characteristics, and then create genetic linkages between them.

For the regional avulsion of Tc1 and the local avulsion of Tc2 that occurred in the early evolution stage of TCs, the former completely changed the channel fairways (Fig. 4A), while the latter only had a small influence on the channel route (Fig. 4B). Such differential effects of avulsion events on the channel-route shifting reflect a reduction in the degree of channel diversion and indicate that the flow courses of TCs were gradually stabilizing with time. On the other hand, quantitative characterization of TCs suggest Tc3, the ultimate product of regional and local avulsions, is significantly different from the early Tc1 and Tc2 (Table 2). Tc3 consists of muti-stage depositional elements and has much larger scale parameters (Table 2), suggesting more profound impacts of flows to the overall channel morphology. Therefore, Tc3 are more mature compared with Tc1 and Tc2 (Posamentier and Kolla, 2003; Gee et al., 2007; Kane and Hodgson, 2011; Maier et al., 2013). It could be found there is a synchronization between channel-course stabilization and channel maturity in the early evolution stage of submarine channels. That is, only after attaining a stable flow course, can submarine channels go through a significant evolution and reach equilibrium with the corresponding gravity flows. However, if the course is highly unstable, high-degree channel diversion, for example, the regional avulsion, tends to occur and prevents channels from continuously developing. This is the case with Tc1, which failed to develop further following the diversion of entire flow discharges towards southwest.

In the late evolution stage of TCs, Tc3 had already gone through a significant evolution after attaining its stable course by avulsing (Fig. 8). However, it must be noted that the continuous development and maturing, in turn, would lead to the instability in deep-water systems, because there are eventually shorter and more efficient routes for gravity flows to reach their base level (Kolla, 2007; Armitage et al., 2012; Maier et al., 2013; Dorrell et al., 2015). Therefore, four bank crevasses of Tc3 occurred when the channel-instability reached the avulsion-threshold condition in the late evolution stage (Fig. 8). Unlike the early regional avulsion and local avulsion that reset the process of
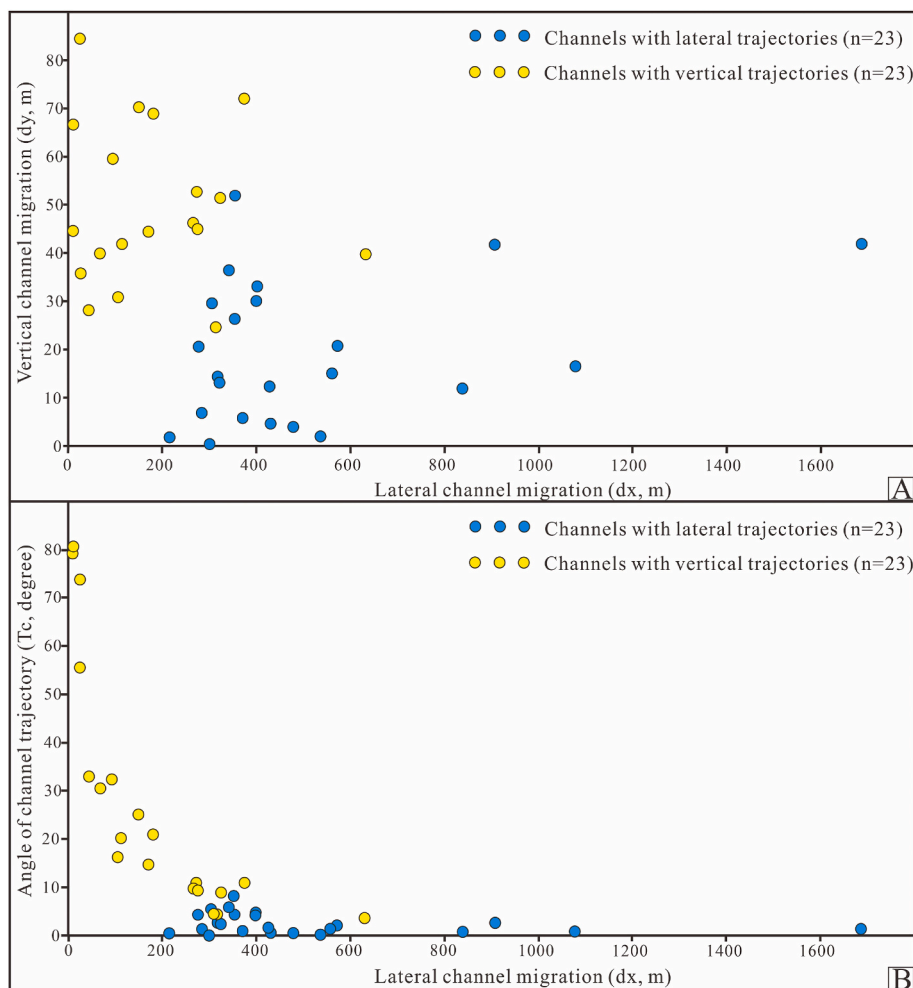
Fig. 11. Scatterplots of dx vs. dy (A) and of dx against T_c (B) for Tc3 channel elements with lateral and vertical trajectories (blue and yellow dots, respectively). All data points in this figure are measured from uninterpreted seismic sections shown in this paper where blue and yellow dots respectively represent the channel-thaweg positions of amalgamated and aggradational channel elements of Tc3. (For interpretation of the references to color in this figure legend, the reader is referred to the Web version of this article.)

channel reaching equilibrium with the corresponding gravity flows and resulted in different maturity in adjacent channels, these bank crevasses triggered the formation of crevasse splays and had no impact on flow course shifting. This is because in the very late stage of channel evolution, avulsive flows originated from levee breaches do not have enough energy to deepen and enlarge the crevasse throats so as to completely divert into another direction. The avulsion process, therefore, was forced to be aborted prior to the whole system shut-off. It is conceivable that if the avulsion process continued, these breaches would capture all gravity flows from Tc3 and a single dominant channel would developed. Such explanations are consistent with the conclusions of Slingerland and Smith (2004) that avulsion sites commonly begin as crevasses, and of Ortiz-Karpf et al. (2015) that crevasse splays form at the start of an avulsion cycle.

7.2. Relating different avulsion events to architectural variations of submarine channels

As stated above, both of the avulsion event and the architectural style of TCs show systematically variations during the evolution process. Therefore, we can make such an assumption that there is an intrinsic connection between them. To prove this hypothesis, we first need to (1) exam the coupling relationship between those different avulsions and varied architectural styles, and then (2) discuss the interactions between them.

If channel architectural styles and avulsion behaviors are really coupled, the most convincing test would be a demonstration that the specific avulsion behavior occurred concurrently with a certain kind of architectural style. Through a series of isochronous slices extracted from different evolution times of TCs (Figs. 4 and 8), we did find a correspondence between channel avulsion events and architectural styles. More specifically, the regional avulsion occurred at a very early time is related to individual-channel development (Fig. 4A). The subsequent local avulsion corresponds to the amalgamated stacking of channel elements (Fig. 4B), and at the late stage of channel evolution, bank crevasses and aggradational channel elements had co-occurred (Fig. 8A and B).

According to the review of Kolla (2007), the occurrence of any form of avulsion event relies on a high degree of channel instability. Channel sinuosity increase and lengthening, channel thalweg aggradation and decrease in relief, differential channel fill, slumping, and channel plugging are all important processes or events leading to intrinsically unstable channel courses and subsequent avulsions (Posamentier and Kolla, 2003; Kolla, 2007; Armitage et al., 2012; Brunt et al., 2013; Morris et al., 2014). In this study, the three types of channel architecture patterns are respectively associated with one or two of those processes or events. First, for the architectural style of individual-channel development, Tc1 mainly developed sinuosity (with a maximum value of 2.17), and the corresponding avulsion occurred at the vertex of a sharp bend (Fig. 4). Second, for the channel elements stacked in a disorganized amalgamation pattern, deposition from successive gravity flows favor a completely fill in the bank-full form and cause a certain degree of channel plugging (Posamentier and Kolla, 2003, Mchargue et al., 2011). When this occurs at the end of a turbidity current event, the following turbidity currents tend to avoid the paths of the previous flows and thus stand a good chance to avulse. Lastly, for the aggradational stacking
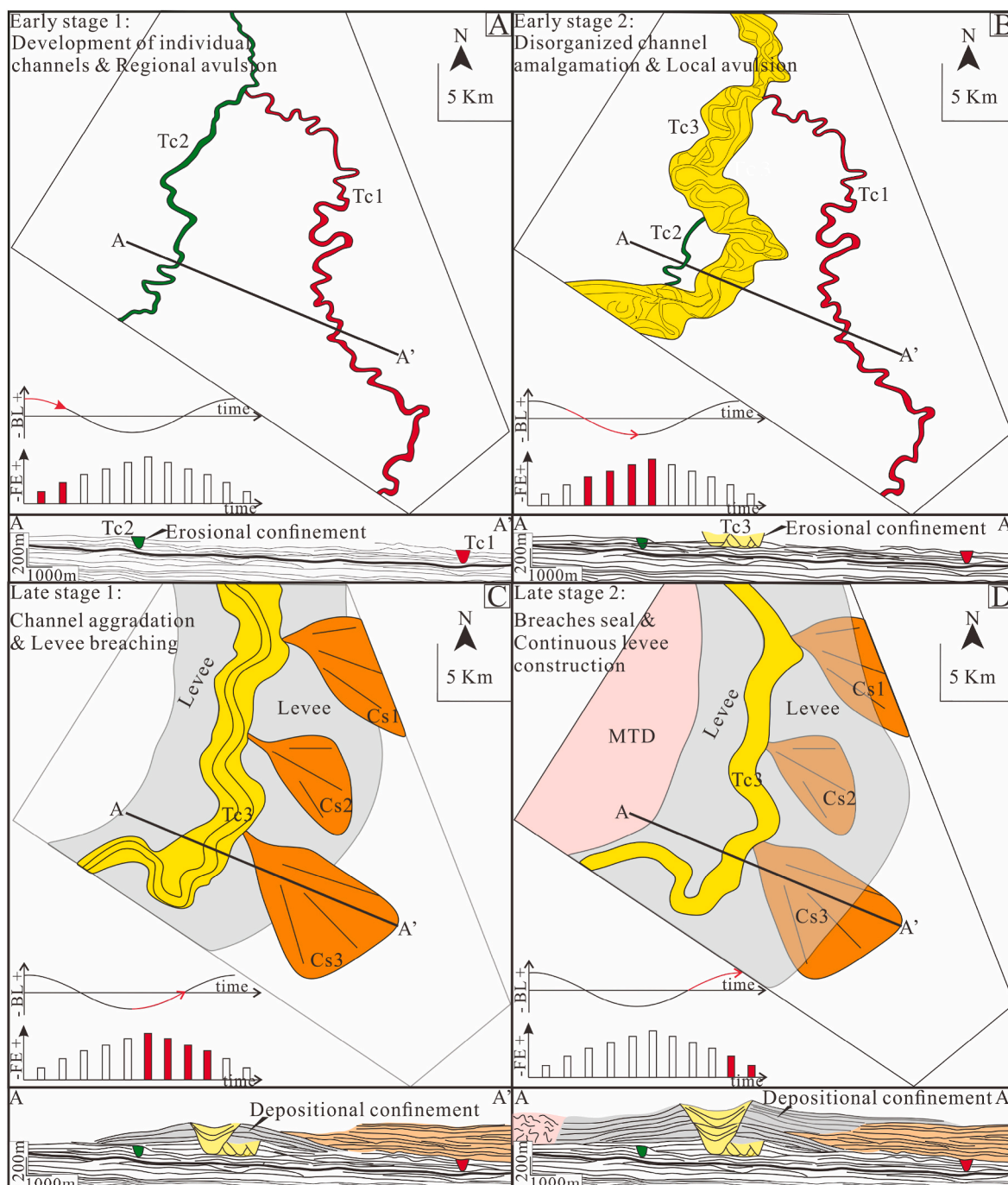
Fig. 12. Sketch diagrams (respectively mapped from Slice 1, 2, 5, and 6) showing the four-stage evolution of target channels within the context of a waxing-waning cycle of flow energy. (A) During Early stage 1, i..e. the onset of flow-energy rise, the individual channel had continuously developed and caused the occurrence of regional avulsion. (B) During Early stage 2, with the further going up of flow energy, submarine channels started to migrate laterally and disorganizedly, giving rise to a amalgamated stacking pattern and a local avulsion phenominenon. (C) In Late stage 1, the flow energy started to decrease and correspondingly, pronounced levee deposits, aggradational channel succession, bank crevasses, and resultant crevasse splays had collectively showed up. (D) For Late stage 2 towards the end of the deep-water episode, the breached levees had gradually sealed and subsequently, the continuously developed levees had draped the east-bank crevasse splays, with only the most distal parts exposed. Note that the actual relative durations and amplitudes of the waxing and waning phases are unkown and for simplicity, the cycle is displayed in a symetrical manner. BL = Base level; FE = Flow energy.

pattern, successive turbidity currents tend to erode and subsequently fill channels incompletely (Posamentier and Kolla, 2003, Mchargue et al., 2011). Such in-channel aggradation and resultant reduction of channel relief will also increase the possibility of avulsion.

7.3. Temporal-spatial evolution of submarine channels within the context of a waxing-waning cycle of flow energy

The avulsion events and architectural styles of submarine channels are influenced by both the extra-basinal (allogenic) controls, such as climates, sea levels, and tectonics, and the intra-basinal (autogenic) factors, such as substrate topographies and gradients (Kolla, 2007; Picot

et al., 2016; Groenenberg et al., 2009, 2010, 2010; Gong et al., 2021). However, due to the limitation of the study area and insufficient data sets, conducting analysis for these specific controls is not possible. We, therefore, just roughly place the whole development process of TCs within the context of the sequence-stratigraphic concept and the resultant waxing-waning cycle of the flow energy. Such a flow-energy cycle is interpreted to result from systematic, and presumably gradual, changes in frequencies, volumes, and sand contents of turbidity flows through time. According to the classic sequence stratigraphy model (Vail et al., 1977; Posamentier et al., 1992; Posamentier and Kolla, 2003), gravity flows into deep-water areas tend to increase in frequencies, magnitudes, and sand contents when base level falls and decrease when the base level rises. As shown in Fig. 12, TCs in total underwent four evolution stages, which respectively correspond to different portions of the waxing-waning flow-energy cycle and to distinct channel avulsion events and architecture styles.

In Early stage 1, the onset of base-level fall increased the incidence of slope failure and associated sediment gravity flows. Consequently, during this earliest waxing portion of the flow-energy cycle, small-volume and low-frequency turbidity currents only caused the formation of individual channels (Tc1 and Tc2), and corresponded to the occurrence of the regional avulsion (Fig. 12A). In Early stage 2, as the base level further fell, the progress of the waxing energy phase continued. Flows tended to be characterized by increasing discharges, sand contents, and event frequencies and thus, are highly erosive with respect to channels inherited from earlier flow events. Accordingly, channels during this period were only confined by the erosional relief (erosional channel walls) and tended to shift laterally and randomly, causing local avulsion and subsequent amalgamated stacking of channel elements. (Fig. 12B). During Late stage 1, as the rise of the base level, terrigenous sediments were progressively sequestered inboard of the shoreline, decreasing the total volume and sand content of gravity flows exported into deep-water areas. As a consequence of such progressively smaller and muddier flow events, levee deposits significantly accumulated, providing high depositional relief. Those depositional relief, coupled with the inherited erosional confinement, facilitated the transition in channel architecture style from amalgamation to aggradation and the subsequent formation of bank crevasses (Fig. 12C). In Late stage 2, as the base level peaked, the waning energy phase continued until the end of the deep-water episode, during which the time-averaged composition of repeated flows became even muddier. Therefore, the deposition of mud-rich sediments in overbank areas continuously proceeded and healed the breaches. Those levee deposits occurred at the eve of the whole system shut-off had draped the previous crevasse splays, with only the most distal part being exposed (Fig. 12D).

8. Conclusion

(1) TCs consist of three independent submarine channels (Tc1-Tc3) and during its evolution process, both avulsion events and architectural styles exhibit systematical variations. On the one hand, regional avulsion, local avulsion, and bank crevasse sequentially occurred, which respectively totally changed, slightly adjusted, and barely impacted the channel pathways. On the other hand, there is also a transition in channel architectural styles from individual-channel development through amalgamated stacking to aggradational stacking.

(2) Different avulsion events played important roles in the architectural evolution of TCs. The regional avulsion of Tc1 and the local avulsion of Tc2 occurred in the early evolution process, through which TCs attained stable flow routes and then went through a significant evolution, forming the high-maturity Tc3. The bank crevasses of Tc3, however, occurred in the late evolution process when the whole system was already starting to shut-off, thus interrupting the avulsion process and leaving the deposits of crevasse splays in the proximal overbank setting.

(3) There is a coupled relationship between channel avulsion events and architectural styles. Regional avulsion, local avulsion, and bank crevasse seem to be contemporaneous with individual-channel development, amalgamated stacking and the aggradational stacking, respectively. Moreover, those three kinds of channel architecture patterns can lead to the intrinsically unstable channel courses to some extent, and thus, are associated with the occurrences of avulsion events.

(4) In general, the whole evolution process of TCs can be explained by a waxing-waning cycle of flow energy and accordingly, four main evolution stages can be identified. Early stage 1 and Early stage 2 correspond to the waxing phase of the cycle, during which increasing flow events led to the transition from regional to local avulsion, and in architecture styles from individual-channel development to amalgamated stacking. Late stage 1 and Late stage 2, however, took place during the waning portion of the cycle when flows with smaller volumes and muddier contents favored the construction of overbank deposits, correlating with the aggradational succession of channel elements and the breaching and subsequent sealing of levee breaches.

References

Abreu, V., Sullivan, M., Pirmez, C., Mohrig, D., 2003. Lateral accretion packages (LAPs): an important reservoir element in deep water sinuous channels. Mar. Petrol. Geol. 20, 631–648.

Alam, M., Alam, M.M., Curray, J.R., Chowdhury, M.L.R., Gani, M.R., 2003. An overview of the sedimentary geology of the Bengal Basin in relation to the regional tectonic framework and basin-fill history. Sediment. Geol. 155, 179–208.

Armitage, D.A., McHargue, T., Fildani, A., Graham, S.A., 2012. Postavulsion channel evolution: Niger Delta continental slope. AAPG Bull. 96, 823–843.

Bastia, R., Das, S., Radhakrishna, M., 2010. Pre- and post-collisional depositional history in the upper and middle Bengal fan and evaluation of deep-water reservoir potential along the northeast Continental Margin of India. Mar. Petrol. Geol. 27, 2051–2061.

Brunt, R.L., Di Celma, C.N., Hodgson, D.M., Flint, S.S., Kavanagh, J.P., Van der Merwe, W.C., 2013. Driving a channel through a levee when the levee is high: an outcrop example of submarine down-dip entrenchment. Mar. Petrol. Geol. 41, 134–145.

Bull, S., Cartwright, J., Huuse, M., 2009. A review of kinematic indicators from masstransport complexes using 3D seismic data. Mar. Petrol. Geol. 26, 1132–1151.

Clark, I.R., Cartwright, J.A., 2009. Interactions between submarine channel systems and deformation in deepwater fold belts: examples from the Levant Basin, Eastern Mediterranean Sea. Mar. Petrol. Geol. 26, 1465–1482.

Curray, J.R., Moore, D.G., 1971. Growth fo the Bengal deep-sea fan and denudation in the Himalayas. Geol. Soc. Am. Bull. 82, 563–572.

Curray, J.R., 1991. Possiblegreenschist metamorphism at the base of a 22-km sedimentary section. Bay of Bengal: Geology 19, 1097–1100.

Curray, J.R., 1994. Sediment volume and mass beneath the Bay of bengal. Earth Planet Sci. Lett. 125, 371–383.

Curray, J.R., Emmel, F.J., Moore, D.G., 2003. The Bengal Fan: morphology, geometry, stratigraphy, history and processes. Mar. Petrol. Geol. 19, 1191–1223.

Damuth, J.E., Kolla, V., Flood, R.D., Kowsmann, R.O., Monteiro, M.C., Gorini, M.A., Palma, J.J.C., Belderson, R.H., 1983a. Distributary channel meandering and bifurcation patterns on the Amazon deep-sea fan as revealed by long-range side-scan sonar (GLORIA). Geology 11, 94–98.

Damuth, J.E., Kowsmann, R.O., Flood, R.D., Belderson, R.H., Gorini, M.A., 1983b. Age relationships of distributary channels on Amazon deep-sea fan: implications for fan growth pattern. Geology 11, 470–473.

Deptuck, M.E., Steffens, G.S., Barton, M., Pirmez, C., 2003. Architecture and evolution of upper fan channel-belts on the Niger Delta slope and in the Arabian Sea. Mar. Petrol. Geol. 20, 649–676.

Deptuck, M.E., Sylvester, Z., Pirmez, C., O'Byrne, C., 2007. Migration–aggradation history and 3-D seismic geomorphology of submarine channels in the Pleistocene Beninmajor Canyon, western Niger Delta slope. Mar. Petrol. Geol. 24, 406–433.

Dorrell, R.M., Burns, A.D., McCaffrey, W.D., 2015. The inherent instability of leveed seafloor channels. Geophys. Res. Lett. 42, 4023–4031.

Droz, L., Marsset, T., Ondréas, H., Lopez, M., Savoye, B., Spy-Anderson, F.L., 2003. Architecture of an active mud-rich turbidite system: the Zaire Fan (Congo–Angola margin southeast Atlantic): results from ZaïAngo 1 and 2 cruises. AAPG Bull. 87, 1145–1168.

Flood, R.D., Manley, P.L., Kowsmann, R.O., Appi, C.J., Pirmez, C., 1991. Seismic facies and late quaternary growth of Amazon submarine fan. In: Weimer, P., Link, M.H. (Eds.), Seismic Facies and Sedimentary Process of Submarine Fans and Turbidite Systems. Springer, New York, pp. 415–433.

France-Lanord, C., Schwenk, T., Klaus, A., 2014. Expedition 354 scientific prospectus: bengal fan. International Ocean Discovery Program.

Gee, M.J.R., Gawthorpe, R.L., Bakke, K., Friedmann, S.J., 2007. Seismic geomorphology and evolution of submarine channels from the Angolan continental margin. J. Sediment. Res. 77, 433–446.

Gong, C.L., Wang, Y.M., Hodgson, D.M., Zhu, W.L., Li, W.G., Xu, Q., Li, D., 2014. Origin and anatomy of two different types of mass-transport complexes: a 3D seismic case study from the northern South China Sea margin. Mar. Petrol. Geol. 54, 198–215.

Gong, C., Peakall, J., Wang, Y., Wells, M., Xu, J., 2017. Flow processes and sedimentation in contourite channels on the northwestern South China Sea margin: a joint 3D seismic and oceanographic perspective. Mar. Geol. 393, 176–193.

Gong, C., Li, D., Qi, K., Xu, H., 2020. Flow processes and sedimentation in a straight submarine channel on the Qiongdongnan margin, northwestern south China sea. J. Sediment. Res. 90, 1372–1388.

Gong, C., Steel, J.R., Qi, K., Wang, Y., 2021. Deep-water channel morphologies, architectures, and population densities in relation to stacking trajectories and climate states. GSA Bulletin 133, 287–306.

Groenenberg, M.R., Sloff, K., Weltje, G., 2009. A high-resolution 2-DH numerical scheme for process-based modeling of 3-D turbidite fan stratigraphy. Comput. Geosci. 35, 1686–1700.

Groenenberg, M.R., Hodgson, M.D., Prelat, A., Luthi, M.S., Flint, S., 2010. Flow-depositional interaction in submarine lobes: insights from outcrop observations and realizations of a process-based numerical model. J. Sediment. Res. 80, 252–267.

Harrowfield, G., 2015. Mass transport complexes of the Rakhine Basin, Myanmar – deepwater examples from recent 3D seismic data: SEAPEX Exploration Conference (Abstract).

Heller, P.L., Paola, C., 1996. Downstream changes in alluvial architecture: an exploration of controls on channel stacking patterns. J. Sediment. Res. 66, 297–306.

Hansen, L., Janocko, M., Kane, I., Kneller, B., 2017. submarine channel evolution, terrace development, and preservation of intra-channel thin-bedded turbidites: mahin and avon channels, offshore Nigeria. Mar. Geol. 383, 146–167.

Hodgson, D.M., Bernhardt, A., Clare, M., Silva, A., Fosdick, J., Mauz, B., et al., 2018. Grand challenges (and great opportunities) in sedimentology, stratigraphy, and diagenesis research. Front. Earth Sci. 6, 173.

Kane, I.A., Hodgson, D.M., 2011. Sedimentological criteria to differentiate submarine channel levee subenvironments: exhumed examples from the rosario Fm. (Upper cretaceous) of baja California, Mexico, and the fort Brown Fm. (Permian), karoo basin, S. Africa. Mar. Petrol. Geol. 28, 807–823.

Kenyon, N.H., Amir, A., Cramp, A., 1995. Geometry of the younger sediment bodies of the Indus Fan. In: Pickering, K.T., Hiscott, R.N., Kenyon, N.H., Lucchi, F.R., Smith, R.D.A. (Eds.), Atlas of Deep Water Environments. Springer, Netherlands, pp. 89–93.

Kolla, V., 2007. A review of sinuous channel avulsion patterns in some major deep-sea fans and factors controlling them. Mar. Petrol. Geol. 24, 450–469.

Kolla, V., Coumes, F., 1987. Morphology, internal structure, seismic stratigraphy, and sedimentation of Indus Fan. AAPG Bull. 71, 650–677.

Lowe, R.D., Graham, A.S., Malkowski, A.M., Das, B., 2019. The role of avulsion and splay development in deep-water channel systems: sedimentology, architecture, and evolution of the deep-water Pliocene Godavari "A" channel complex, India. Mar. Petrol. Geol. 105, 81–99.

Ma, H., Fan, G., Shao, D., Ding, L., Sun, H., Zhang, Y., Zhang, Y., Cronin, B., 2020. Deep-water depositional architecture and sedimentary evolution in the Rakhine Basin, northeast Bay of Bengal. Petrol. Sci. 17, 598–614.

Maier, K.L., Fildani, A., Paull, C.K., McHargue, T.R., Graham, S.A., Caress, D.W., Talling, P., 2013. Deep-sea channel evolution and stratigraphic architecture from inception to abandonment from high-resolution Autonomous Underwater Vehicle surveys offshore central California. Sedimentology 60, 935–960.

Manley, P.L., Flood, R.D., 1988. Cyclic deposition within Amazon deep-sea fan. AAPG Bull. 72, 912–925.

Mchargue, T., Pyrcz, M.J., Sullivan, M.D., Clark, J.D., Fildani, A., Romans, B.W., Covault, J.A., Levy, M., Posamentier, H.W., Drinkwater, N.J., 2011. Architecture of turbidite channel systems on the continental slope: patterns and predictions. Mar. Petrol. Geol. 28, 728–743.

Moscardelli, L., Wood, L., Mann, P., 2006. Mass-transport complexes and associated processes in the offshore area of Trinidad and Venezuela. AAPG Bull. 90, 1059–1088.

Morris, E.A., Hodgson, D.M., Brunt, R.L., Flint, S.S., 2014. Origin, evolution and anatomy of silt-prone submarine external levées. Sedimentology 61, 1734–1763.

Nakajima, T., Kneller, B.C., 2013. Quantitative analysis of the geometry of submarine external levees. Sedimentology 60, 877–910.

Oluboyo, A.P., Gawthorpe, R.L., Bakke, K., Hadler-Jacobsen, F., 2014. Salt tectonic controls on deep-water turbidite depositional systems: Miocene, southwestern lower Congo basin, offshore Angola. Basin Res. 26, 597–620.

Ortiz-Karpf, A., Hodgson, D.M., McCaffrey, W.D., 2015. The role of mass-transport complexes in controlling channel avulsion and the subsequent sediment dispersal patterns on an active margin: the Magdalena Fan, offshore Colombia. Mar. Petrol. Geol. 64, 58–75.

Picot, M., Droz, L., Marsset, T., Dennielou, B., Bez, M., 2016. Controls on turbidite sedimentation: insights from a quantitative approach of submarine channel and lobe architecture (late Quaternary Congo Fan). Mar. Petrol. Geol. 72, 423–446.

Piper, D.J.W., Normark, W.R., 1983. Turbidite depositional patterns and flow characteristics, navy submarine fan, California borderland. Sedimentology 30, 681–694.

Piper, D.J.W., Normark, W.R., 2001. Sandy fans: from Amazon to hueme and beyond. AAPG Bull. 85, 1407–1438.

Pirmez, C., Hiscott, R.N., Kronen, J.D., 1997. Sandy turbidite successions at the base of channel-levee systems of the Amazon Fan revealed by FMS logs and cores: unraveling the facies architecture of large submarine fans. In: Flood, R.D., Piper, D.J.W., Klaus, A., Peterson, L.C. (Eds.), Proceedings of the Ocean Drilling Program, Scientific Results, vol. 155, pp. 7–33.

Posamentier, H.W., Allen, G.P., James, D.P., Tesson, M., 1992. Forced regressions in a sequence stratigraphic framework: concepts, examples, and exploration significance: American Association of Petroleum Geologists. Bulletin 76, 1687–1709.

Posamentier, H.W., Kolla, V., 2003. Seismic geomorphology and stratigraphy of depositional elements in deep-water settings. J. Sediment. Res. 73, 367–388.

Schwenk, T., Spieß, V., 2009. Architecture and stratigraphy of the Bengal Fan as response to tectonic and climate revealed from high-resolution seismic data. In: Kneller, B.C., Martinsen, O.J., McCaffrey, B. (Eds.), External Controls on Deep-Water Depositional Systems, vol. 92. Special Publication - SEPM (Society of Sedimentary Geologists), pp. 107–131.

Slingerland, R., Smith, N.D., 2004. River avulsions and their deposits. Annu. Rev. Earth Planet Sci. 32, 257–285.

Smith, N.D., Cross, T.A., Dufficy, J.P., Clough, S.R., 1989. Anatomy of an avulsion. Sedimentology 36, 1–23.

Sun, H., Fan, G.Z., Lyu, F.L., Xu, Z.C., Ma, H.X., 2011. Sedimentary characteristics of pliocene slope channel complexes in theRakhine Basin. offshore Myanmar: ActaSedimentologicaSinica 29, 695–703.

Tang, P., Lv, F., Fan, G., Shao, D., Wang, X., Sun, H., Li, L., 2013. A preliminary study on the late cenozoic structural characteristics of the arakan fold belt, Bay of bengal. Acta Geol. Sin. 87, 1013–1020 (in Chinese).

Vail, P.R., Mitchum, R.M.J., Thompson, S., 1977. Seismic stratigraphy and global changes of sea level, Part 3: relative changes of sea level from coastal onlap. In: Payton, C.E. (Ed.), Seismic Stratigraphy-Application to Hydrocarbon Exploration. American Association of Petroleum Geologists, Oklahoma, pp. 63–82.

Wang, X.L., Lv, F., Fan, G., Shao, D., Sun, H., Tang, P., 2013. Structural characteristics and evolution of Rakhine Basin, Bay of bengal. J. Chengdu Univ. Technol. (Sci. Technol. Ed.) 40, 424–430 (In Chinese).

Weber, E.M., Wiedicke-Hombach, M., Kudrass, H.R., Erlenkeuser, H., 2003. Bengal Fan sediment transport activity and response to climate forcing inferred from sediment physical properties. Sediment. Geol. 155, 361–381.

Yang, S.Y., Kim, J.W., 2014. Pliocene basin-floor fan sedimentation in the Bay of Bengal. Mar. Petrol. Geol. 49, 45–58.

Zhan, L., Guo, B., Yu, Y., 2019. Architectural elements and stratigraphy of a deepwater fan: a case study of the Bengal Fan, Rakhine Basin, offshore Myanmar. Arabian Journal of Geoences 12 (212).

Zhao, X., Qi, K., Liu, L., Gong, C., McCaffrey, D., 2018a. Development of a partially-avulsed submarine channel on the Niger Delta continental slope: architecture and controlling factors. Mar. Petrol. Geol. 95, 30–49.

Zhao, X.M., Qi, K., Liu, L., Xie, T., Li, M.H., Hu, G.Y., 2018b. Quantitative characterization and controlling factor analysis of the morphology of Bukuma-minor Channel on southern Niger Delta slope. Intepret.J. Sub. 6, 57–69.

Zhao, X., Qi, K., Patacci, M., Tan, C., Xie, T., 2019. Submarine channel network evolution above an extensive mass-transport complex: a 3D seismic case study from the Niger delta continental slope. Mar. Petrol. Geol. 104, 231–248.